Electrochimica Acta 511 (2025) 145366

Contents lists available at ScienceDirect

Electrochimica Acta

journal homepage: www.journals.elsevier.com/electrochimica-acta

Influences on the anisotropy in through-mask electrochemical micromachining processes

Leonie Jakob *, Jonas Bartsch

Metallization and Structuring Technologies, Fraunhofer Institute for Solar Energy Systems ISE, Heidenhofstr. 2, 79110 Freiburg, Germany

ARTICLE INFO

Keywords:
Anisotropy
Through-mask EMM
Surface films

ABSTRACT

This contribution studies through-mask electrochemical micromachining (TMEMM) of copper, namely the interplay between current density, electrolyte flow, mask opening width, etch depth, the presence of a wetting agent, and the resulting anisotropy in sodium nitrate electrolyte. Factors strengthening the anisotropy are: High electrolyte flow rate, low overall etch depth and large feature size (150 µm > 100 µm > 50 µm), absence of wetting agent, and moderate current densities (between 20 and 40 A cm^{-2}). A model aiming to explain all the observed interdependencies is elaborated, based on the presence of a supersaturated surface film and a local change in dissolution mechanism in dependence on local current distribution and surface film thickness. The thickness of the surface film is greatly influenced by the flow velocity, which in turn depends on the geometry of the cavity and, therefore, opening width and etch depth. In the presence of a wetting agent the differences in surface film thickness are leveled out, which results in less anisotropic etching.

1. Introduction

As already indicated by several publications, through-mask electrochemical micromachining (TMEMM) is a promising technique for thin film metal patterning. [1–3] The high etching rates and the non-hazardous chemicals make it a fast and environmentally friendly process. Especially the patterning of copper is of interest for applications in the printed circuit board industry. [4,5]

In many applications, achieving highly anisotropic metal etching is desired, allowing for narrow and closely arranged patterns. This is often quantified by the so-called etch factor (EF), which describes the ratio of etch depth to under etching under the resist mask (Eq. (1)). The calculation is visualized in Fig. 1.

$$EF = \frac{etch\ depth\ d}{under\ etching\ u} = \frac{etch\ depth\ d}{\frac{final\ opening\ width - initial\ mask\ opening\ width}{2}} \quad (1)$$

There are several publications investigating the influence of different process conditions (e.g., current density, electrolyte flow, mask thickness, mask wall angle) on the anisotropy by conducting simulations and experiments. However, it is difficult to compare the obtained results and extract universally valid statements from these publications as the basic conditions vary greatly. Especially the etch depth and the relation of current density / voltage to electrolyte flow are often unknown or varying. This is most likely the main reason for contradictory results regarding the influence of the current density / potential on the anisotropy of the etching process. [6,7] The authors agree regarding the negative impact of a very small mask aspect ratio [8–10] (AR_{mask} = height / width of mask opening) and large etch depth. [8,9,11] The (often varying) etch depth, together with the feature size, define another aspect ratio ($AR_{opening}$ = total feature depth (mask + etch depth) / mask opening size), which is very scarcely considered.

Besides the physico-chemical influencing factors named above, the electrolyte has a large impact on the process results. The most common electrolyte applied for TMEMM processes on different metals is sodium nitrate. It is often preferred due to the superior surface finishing properties and leveling effects. Despite many years of application of these processes, there is surprisingly little insight into the mechanisms of electrolyte-metal interaction. One realistic theory to explain these effects is provided by Lohrengel et al. [12,13] They postulated the formation of supersaturated surface films made of metal nitrates, exhibiting reduced conductivity and increased viscosity. These are formed due to mass transport limitations at and above the limiting current. [14] Lohrengel et al. provide several experiments and arguments as to why the "compact-salt-film-mechanism" proposed earlier by Datta, Landolt and others [15] is rather improbable. [13] For other electrolytes the formation of such supersaturated surface films has been postulated already

* Corresponding author.
E-mail addresses: leonie.jakob@ise.fraunhofer.de (L. Jakob), jonas.bartsch@ise.fraunhofer.de (J. Bartsch).

https://doi.org/10.1016/j.electacta.2024.145366
Received 6 May 2024; Received in revised form 25 October 2024; Accepted 15 November 2024
Available online 22 November 2024
0013-4686/© 2024 The Author(s). Published by Elsevier Ltd. This is an open access article under the CC BY license (http://creativecommons.org/licenses/by/4.0/).

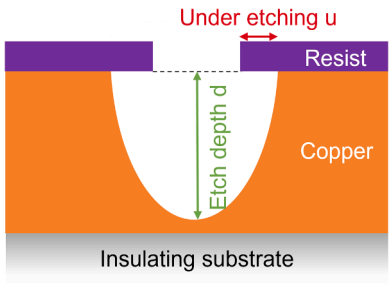


Fig. 1. Graphical illustration of etch factor definition.

in the 1980s. [16]

Alkire already connected the presence of a "surface film" to increased anisotropy, dealing with stainless steel in sulfuric acid. [17] Nevertheless, the explanation for the observed effect based on the presence of the surface film is missing. The explanation for the increased anisotropy is solely based on flow patterns within the cavities. The same applies to an evaluation conducted by Dikusar et al., which focuses on the analysis of stainless steel in acidic NaCl solution. [18] They observed a sharp maximum of the anisotropy of the etching process right at the limiting current density. They explain the observed behavior also by mass transport conditions within the cavity. In both publications, cavities with rather low $AR_{opening}$ are investigated. These publications are valuable preliminary work for postulating a hypothesis on the exact cause of the observed anisotropy.

In this publication, we aim to extend the provided results and elaborate on more comprehensive explanations. This is done by presenting consistent results on the anisotropy of TMEMM processes on copper in a sodium nitrate electrolyte. Relevant influencing factors such as current density, electrolyte flow velocity, etch depth, and mask opening width are varied while simultaneously keeping other influencing factors (mask thickness, mask wall angle, setup…) fixed. Comprehensive hypotheses for the presented results are provided, which are supported by many of the experimental findings. This publication therefore contributes to a deeper understanding of the TMEMM process in general.

2. Experimental

A setup providing a shearing electrolyte flow, as introduced in [5], was used for all experiments. Pure copper sheets were used as cathode and were placed in a distance of 5.5 mm to the workpiece. Thin copper sheets mounted on insulating FR-4 substrates, covered by a patterned resist mask (30 µm thick), were used as substrates. The copper thickness was 90 (Sections 3.2.1 and 3.2.3) or 160 µm (Section 3.2.2). One sample consisted of a line of 9 equal openings with 5 mm spacing, as depicted in Fig. 2. The single openings have a size of 100 µm x 2 mm (if not stated differently). Sodium nitrate (2.35 M, 127 mS cm^{-1}, room temperature, pH 7) was used as the electrolyte. The applied current density, electrolyte flow, etch time, and opening width are specified separately. The polarization curves were measured with a scan rate of 2 V s^{-1} in the applied setup by linearly increasing the cell voltage from 0 – 30 V and measuring the resulting current. The tool used was an EA-PS3080–20C from ElektroAutomatik and features a time resolution of 100 ms. In these experiments, the surface was pretreated by a short pre-pulse (10 V, 1 s). This procedure cleaned and activated the copper surface, which led to more reproducible results.

The samples were analyzed by 3D-confocal laser microscopy to measure etch depth and width of the cavities, as described in [5]. Knowing the initial mask opening width allows the calculation of the EF. Details on the performed CFD-simulations are given in the supporting information.

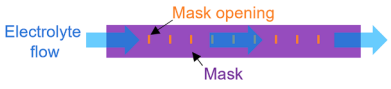


Fig. 2. Schematic drawing of sample and flow direction. Purple: resist mask; blue: electrolyte; orange: copper.

3. Results and discussion

3.1. Preliminary results

3.1.1. Polarization curves

The current density-voltage behavior for our setup/sample configuration (copper, 2.35 M $NaNO_3$, 100 µm openings) is depicted in Fig. 3. The general shape is similar to the curve published by Datta et al. [19] for a recessed anode. The curve can be divided into three parts: a rise of the current density at low voltages (part I), a plateau region with constant current density at intermediate voltages (part II), and a second steep rise at high voltages (part III). Only small differences in the limiting current density were obtained for different electrolyte flow velocities. This can be attributed to the low overall velocity within the cavities (Section 3.1.2). The limiting current density increases by roughly 1 A cm^{-2} per 1 m s^{-1} increase in flow velocity.

3.1.2. Flow conditions

To evaluate the hydrodynamic conditions within the cavities, CFD simulations were conducted. Fig. 4a shows the evolution of the actual flow velocity near the surface (distance depending on simulation mesh, but < 1 µm distance in entire opening) with increasing etch depth within a 100 µm cavity. The arc length corresponds to the path along the metal-electrolyte interface along one cross-section through the etched groove, and consequently increases with increasing etch depth. The results for 50, 150, and 5000 µm cavities are given in the supporting information (Figures S3, S4, and S5). The absolute flow rates, as well as the absolute differences between 2, 3, and 4 m s^{-1}, decrease when the etch depth increases (from black to blue in Fig. 4a). They are significantly lower than the bulk flow rates. An (almost) symmetric distribution results. The maximum flow rate shifts from the center to the edges with increasing etch depth. At high etch depth, the flow velocity is almost homogeneous within the cavity. Fig. 4b shows an exemplary contour plot corresponding to 30 µm etch depth and 3 m s^{-1}. One large recirculating eddy in the center with direct connection to the bulk flow and two small eddies at the edges underneath the mask are observed. Qualitatively, the same behavior is observed for the other flow velocities and etch depths.

It is worth mentioning that the resulting geometries of the etched groves are symmetric in all cases observed in this study, same as the flow rate distributions. No influence of the flow direction was observed.

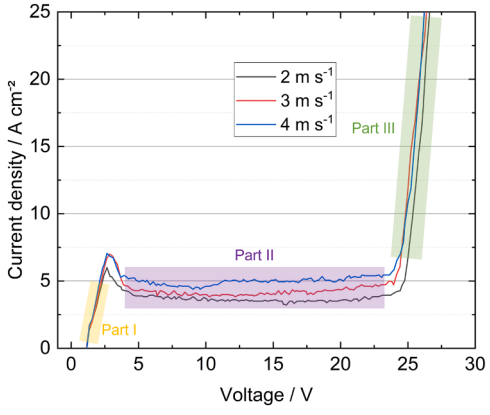


Fig. 3. Obtained current density in dependence of the process voltage for three different flow velocities. The voltage was increased linearly by 2 V s^{-1}.

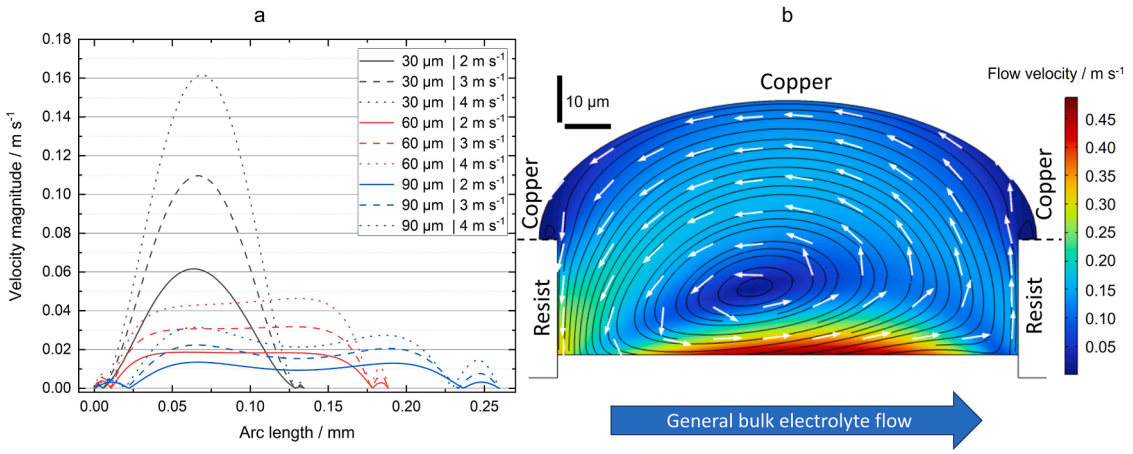


Fig. 4. a) Simulated flow velocities within 100 µm wide cavities at different etch depths (30 – 90 µm, $AR_{opening}$ = 0.6, 0.9 and 1.2) and flow velocities (2 – 4 m s^{-1}). An under etching of 4, 10 and 25 µm was assumed. b) An exemplary contour plot corresponding to 30 µm etch depth and 3 m s^{-1}.

3.2. Parameter variation

In this section, the results obtained from parameter variations are presented. One parameter is varied at a time, while keeping all other parameters constant.

3.2.1. Variation of current density and electrolyte flow

Fig. 5 displays the EF results obtained from a current density and electrolyte flow variation. A total charge of 167 C cm^{-2} has been passed in all experiments, leading to an average etch depth of roughly 60 µm (depending on the current efficiency, valency of the metal dissolution and EF). The voltage at the end of the experiment is given for the different current densities. For 2.5 A cm^{-2} and 5 A cm^{-2}, relatively low processing voltages resulted (corresponding to part I in Fig. 3) for the applied (galvanostatic) processing conditions. The evolution of the voltage is also interesting to consider: at 5 A cm^{-2} at flow velocities of 3 and 4 m s^{-1} the voltage drops from around 24 V to 2 V after a few seconds (shifting the working point from part III to part I). For all other current densities, the voltage increases slightly (1 – 2 V) during the experiment.

All samples show narrow distributions in EF, which result from 288 measurements in total. Two rows of openings were etched for each condition, and 16 measurements were made per each of the nine openings per row. No repeatable trends (e.g., between center and edge) were observed. At low current densities, low EF of around 2 are obtained, while a strong increase in EF is visible with increasing current density until a plateau at around 5 – 6 is reached at intermediate current densities (20 – 40 A cm^{-2}). At very high current densities (> 40 A cm^{-2}) the EF decreases again to values between 3 – 4.

When comparing the results at constant current density with varying electrolyte flow, the EF increases with increasing electrolyte flow velocity at very low (2.5 A cm^{-2}) and very high current density (40 - 100 A cm^{-2}). At 10 and 20 A cm^{-2}, almost no impact of the electrolyte flow is visible, whereas at 5 A cm^{-2}, the EF decreases with increasing flow rate. This effect could be reproduced three times and remained constant. The influence of the flow velocity is stronger at high current densities (≥ 40 A cm^{-2}).

A current density of 40 A cm^{-2} at an electrolyte flow of 4 m s^{-1} leads to a maximum average EF of 6.7 at an etch depth of approx. 60 µm. It is worthy to mention that this EF is comparatively high with respect to earlier publications, [10,20] which underlines the attractiveness of the process regarding anisotropic metal removal. It further motivates to better understand the reasons behind this behavior to control and possibly increase the anisotropy.

3.2.2. Variation of etch depth and opening width

Using the parameter combination of 40 A cm^{-2} and 3 m s^{-1}, an etch depth variation was conducted. This was done for three different mask

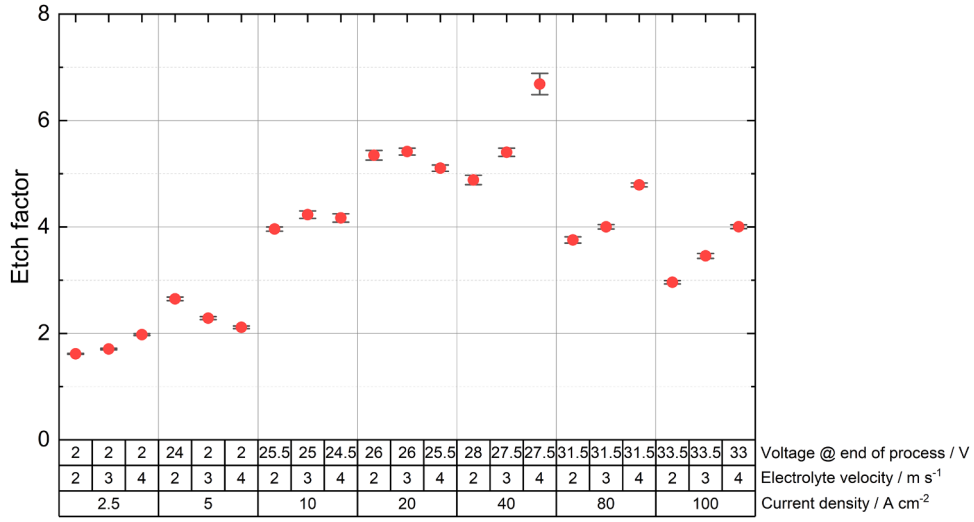


Fig. 5. Obtained EF in dependence of current density and electrolyte velocity. The whiskers include the 95 % confidence interval.

opening widths: 50, 100, and 150 µm. The charges passed for the different etch depths were 83.3; 126.0; 166.7; 208.3; 252.0; 336.0 and 504.0 C/cm^2. The EF results are plotted in Fig. 6 with two different x-axes. Fig. 6a visualizes the differences between the different opening widths depending on the etch depth. Shallow etching results in very high EF > 10 for the 100 µm and 150 µm openings. For etch depths below 40 µm, the analysis of the EF implies a high error, as small differences in under etching result in large deviations in EF. A strong decrease of the EF with increasing etch depth is visible for the 100 µm and 150 µm openings. The general absolute EF level is higher with increasing opening width. For etch depths of up to 50 µm (which includes typical copper layer thicknesses of PCB fabrication), an EF of around 6 can be realized. For the 50 µm openings, a relatively low EF level between 2 – 4 and only a slight decrease with increasing etch depth is obtained.

Fig. 6b displays the same data plotted versus the aspect ratio ($AR_{opening}$) of the final etched groove. This graph illustrates that the observed effects can be attributed to $AR_{opening}$: with increasing $AR_{opening}$, the anisotropy of the etching process is decreasing. Except for very small $AR_{opening}$ (where generally a large scattering of EF is expected/observed) the results for the different opening widths coincide quite well. These results seem to be contradictory to the literature, where a small aspect ratio of the mask (AR_{mask}) is reported to lead to low EF. [8,9,21] Note that AR_{mask} contributes to $AR_{opening}$, especially in the initial phase of the process where etching is still shallow. However, in these publications, the influence of the electrolyte flow is not considered. Further explanations are presented in Section 3.3.

3.2.3. *Influence of wetting agent*

Finally, the influence of a wetting agent (polyalkoxylate) on the anisotropy of the TMEMM process was investigated. Applying the same process conditions as in the previous section (100 µm opening width, 40 A cm^{-2}, 3 m s^{-1}, 167 C cm^{-2}), a wetting agent was added to the electrolyte solution. Experiments at four different wetting agent concentrations have been conducted and are displayed in Fig. 7. A continuous reduction of the EF with increasing wetting agent concentration is observed.

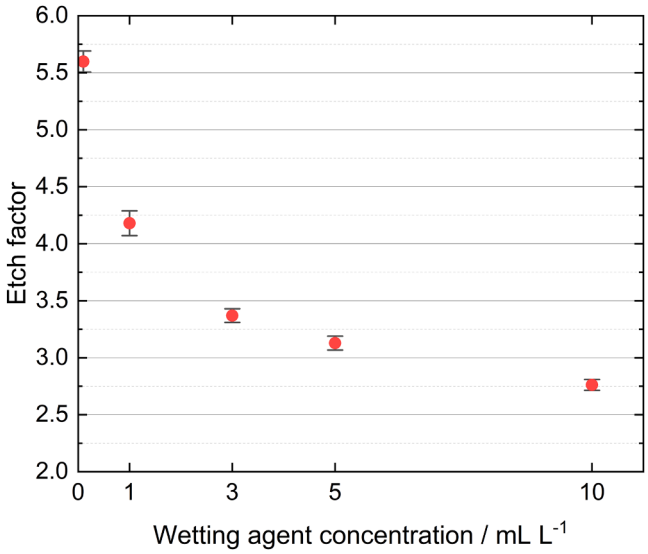


Fig. 7. Resulting EF with increasing wetting agent concentration. The whiskers include the 95 % confidence interval.

Table 1
Summary of the obtained relations between process parameters and anisotropy.

Increase in…	…results in … anisotropy
Current density	increased ↑[1]
Electrolyte flow rate	increased ↑
Aspect ratio	decreased ↓
Wetting agent concentration	decreased ↓

[1] at very high current densities a decrease in anisotropy is obtained.

3.3. *Postulated model*

The previous chapter's results are summarized in Table 1, indicating that the anisotropy in TMEMM processes is influenced by both mass transport effects and current density (distribution). We postulate that these results can be explained by connecting them to the polarization curve and corresponding changes in mechanism. [22]

At **low current densities** below the limiting current at low potentials (part I in Fig. 3), the etching process is directly controlled by the current density, the ohmic drop within the electrolyte (electrolyte resistance) dominates the etching. The electrolyte flow has only a minor influence on the etching results, as mass transport is not limiting at such low dissolution rates. Dissolution occurs without a surface film. At the anode surface, the copper ions are primarily complexed by water and to a lesser extent by nitrate ions. [23] The copper precipitates upon reaching the bulk electrolyte. The results obtained at 2.5 A cm^{-2} belong to this regime. The intrinsic current density distribution is strongly

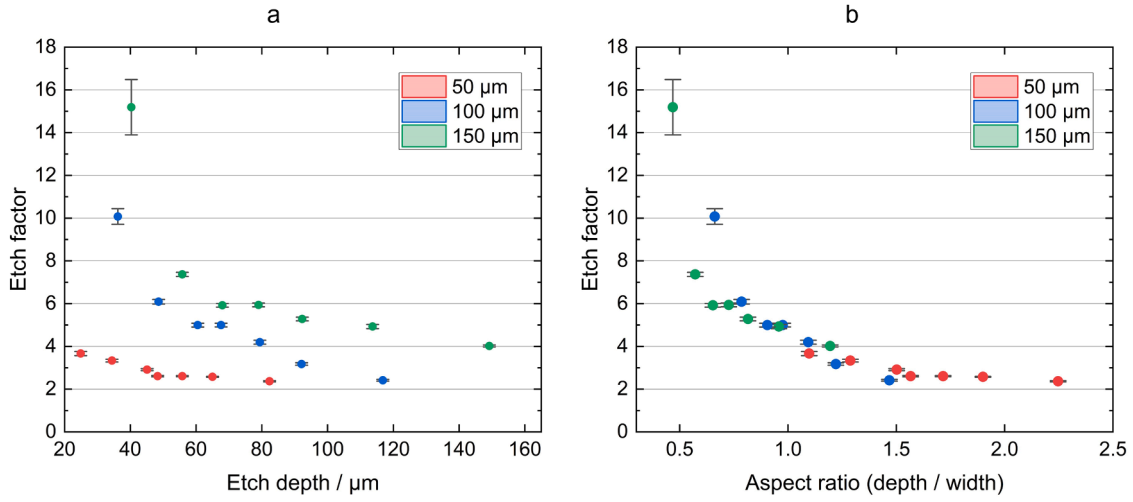


Fig. 6. EF obtained from opening width and etch time variation. a) plot vs. the absolute etch depth b) plot vs. the aspect ratio ($AR_{opening}$) of the opening. The whiskers include the 95 % confidence interval.

influenced by the AR (AR_{mask} is almost equal to $AR_{opening}$ in this situation). [21] For small cavities (AR $\geq$ 0.2) the current density distribution is homogeneous or even exhibits a maximum in the middle of the cavity. This leads to a slightly anisotropic etching with an EF of approx. 2. A strongly reduced mass transport due to unfavorable flow conditions underneath the mask may lead to mass transport limitation in this area already at this low current density and contribute to the slight anisotropy to some extent.

In contrast, larger cavities (AR << 0.2, no results presented in this contribution) exhibit an inhomogeneous current density distribution, with a clear maximum at the edges. [21] Lower EF values are expected from etching at low current densities.

At and above the limiting current density (part II and III in Fig. 3), a supersaturated surface film consisting of copper nitrate, with a very low number of free water molecules, is present. [14] It has an increased resistivity (> 5 times [24]) and viscosity compared to the bulk electrolyte. The large voltage rise in the plateau region results from two factors. The first is the ohmic resistance of the surface film. The second is an apparent resistance due to the depletion of water in the volume of the surface film, which consists almost fully of copper nitrate. For current transport and complexation, diffusion of water into this film must occur, resulting in a diffusion limitation / overpotential. Overlimiting current densities (part III in Fig. 3) become possible above the re-rise voltage by a change in (complexation) mechanism, which occurs as soon as the potential drop at the electrochemical double layer reaches a threshold value. [22] In brief, this mechanism change enables the complexation of copper ions in a matrix of nitrate ions ("solvo-nitration"), thus allowing a process speed independent of water diffusion. It does not occur simultaneously within the entire cavity but results locally from an interplay between the intrinsic electric field distribution and surface film thickness. High field line density and low surface film thickness (high flow velocity) favor the change in mechanism and therefore the re-rise in current density. [22] The more homogeneous the electric field and/or the surface film thickness, the more simultaneous the change in mechanism.

It is this localized change in mechanism that serves as a starting point for the model on anisotropic etching that is presented in the following. For every position within the etch groove, a threshold value (relative to the measured (globally averaged) limiting current density or the re-rise voltage) can be defined, above which the change in mechanism occurs. As it depends on the local field strength *and* the local surface film thickness, it changes with increasing etch depth. Fig. 8 visualizes the assumed / postulated behavior. It shows three distinct polarization curves for three individual positions (red, green, blue) and a superposition of the three curves (black). It seems reasonable that the measured polarization curves in Fig. 3 also display a superposition of several individual polarization curves, stemming from different positions in the etch groove. Depending on the surface position (film thickness and field strength), the additional resistance due to the surface film locally vanishes to a large extent as soon as the change in mechanism happened, as water diffusion overpotential contributes no more.

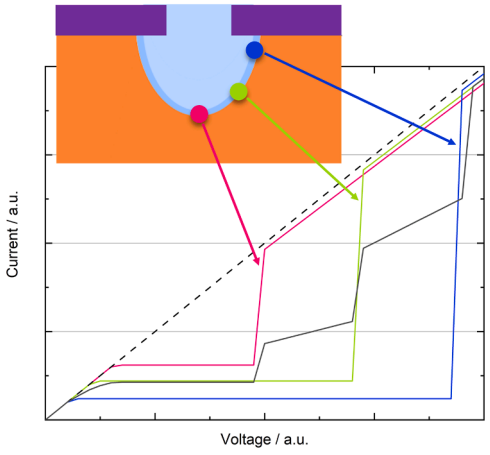


Fig. 8. Schematic visualization of the gradual re-rise in current by the change in mechanism depending on the local current density and electrolyte flow at the different positions within the etch groove. The black curve represents a superposition of the red, green, and blue curve.

With an increasing share of positions with overlimiting current densities a larger part of the cavity is etched with the new mechanism, until at very high voltages/current densities, the entire opening is etched with the new mechanism, resulting again in the intrinsic current density distribution. [22] **We postulate that the anisotropy is strongly connected to the position and the extent of mechanism change at overlimiting current densities.** The position of the mechanism change is then influenced by the field density and the surface film thickness, which are both connected with the cavity to be etched. The surface film thickness is additionally influenced by electrolyte convection and viscosity.

In the following, the flow velocity near the surface will be taken as a direct measure for the surface film thickness. This is a simplification, as other factors (e.g., local temperature) also affect the surface film thickness, but the general trends that shall be illustrated here are mirrored correctly. The current will be considered in units of the limiting current density j_{lim}, as this is the relevant measure for the extent of the change in mechanism.

Fig. 9a qualitatively visualizes the current distribution within a 100 µm wide cavity, **assuming a homogeneous intrinsic current density distribution** and **symmetric flow conditions with the maximum flow rate in the center of the cavity** (which agrees with the results shown in Fig. 4). Below the limiting current density, the etching rate is fully homogeneous (black curve in Fig. 9a, no surface film present). As discussed above, the electrolyte flow does not affect the etching rate in this regime. At the limiting current density, the etch rate distribution reflects the electrolyte flow velocity (red curve in Fig. 9a). Above the limiting current density, the mixed influence of the intrinsic current density distribution and flow velocity becomes apparent, and a partial localized change in mechanism occurs. At the position with the highest flow velocity and therefore the lowest surface film thickness, the change in mechanism occurs first (orange and blue curve in Fig. 9a), resulting in a locally higher current density. This part in the center is etched with the intrinsic current distribution. However, the main part of the cavity, especially at the edges, is still etched at the limiting current density, as the threshold value for the change in mechanism is reached only in a small part in the center. This behavior causes slightly anisotropic etching and corresponds to the results obtained at 5 – 10 A cm^{-2} (Fig. 5).

For higher applied current densities (green and purple curve in Fig. 9a) higher potentials result, which lead to a widening of the region etched with the new mechanism. The current density in the center of the cavity (etched with the new mechanism) increases. The etching rate in the rest of the etch groove still corresponds to the limiting current density. The difference in etch rate between the center (new mechanism) and the edge (old mechanism/limiting current density) increases, leading to higher EF. The trend of increasing EF with increasing current density up to 40 A cm^{-2} is well explained by this behavior (Fig. 5).

Unfortunately, it is not possible to etch to an unlimited depth with a very high level of anisotropy in this case. Gradually, the local etch depth increases, and the local convection is reduced, so mechanism change and local etch rate homogenize. The positions where the change in mechanism occurred are not as clearly defined or static as they appear from the plot. They fluctuate slightly and become blurred due to changes in local flow conditions and etch depths. Nevertheless, the qualitative behavior can be extracted from the curves in Fig. 9.

When the current density is increased further (yellow curve in Fig. 9a), the ratio of the current density between the middle and edge still increases. But, as the part of the cavity etched with the new mechanism approaches the edges, the faster etching near the edges

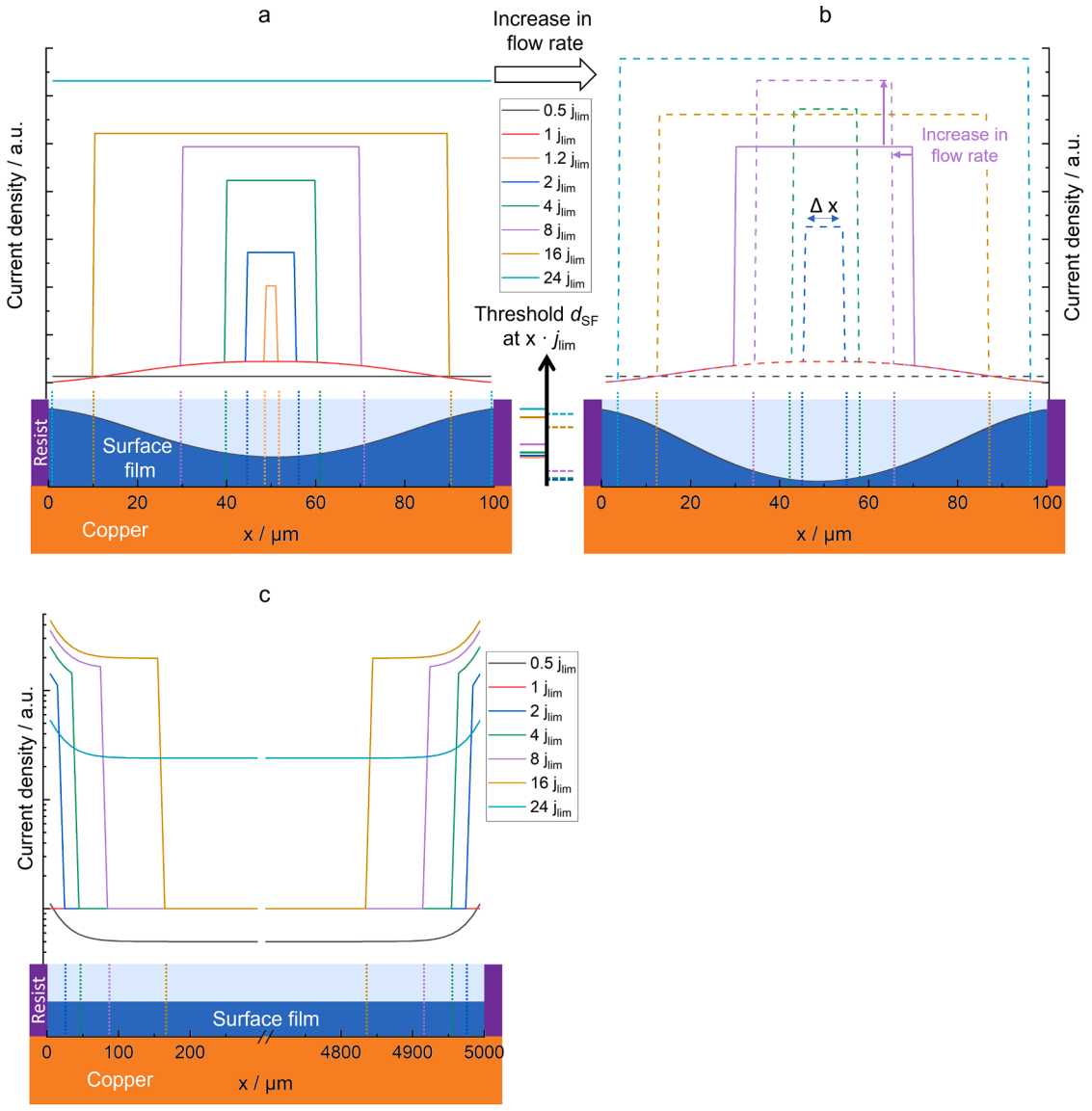


Fig. 9. Visualization of the qualitative current distribution within a 100 µm (a and b) and a 5000 µm (c) cavity in dependence of the applied current density (relative to the limiting current density j_{lim}) for low (a) and high (b) flow rates. a) and b) A fully homogeneous intrinsic current density distribution (black curve) and symmetric flow conditions with higher flow rates in the center of the cavity (corresponding roughly to the red curves in Fig. 4) were assumed. The solid purple curve in b) equals the one in a) and is shown to indicate the decrease in Δx due to the increase in flow rate. c) A fully homogeneous flow velocity (corresponding roughly to Figure S5 in SI) and an intrinsically higher current density at the edges [21,22] (black curve) was assumed. The bottom parts visualize the actual surface film thickness distribution within the cavity and the corresponding threshold values at given relative current density. In the situations corresponding to the black curves no surface film is present.

results in less directed and less anisotropic etching. This fits well with the decreasing anisotropy at current densities > 40 A cm^{-2} (Fig. 5). At very high current densities (cyan curve in Fig. 9a), the mechanism changed throughout the entire cavity, resulting again in the intrinsic current distribution. Therefore, it is expected that an EF level similar to that at very low current densities will be reached in this high current density regime.

From this model, there are two possibilities yielding an increase in anisotropy at given current density (distribution). The limiting current density in the center may be significantly increased compared to the edges (first possibility), or the change in mechanism occurs in a narrower part in the center of the opening, resulting in a higher absolute current density in this part and a more localized faster etching (second possibility).

With increasing bulk flow velocity, the **flow velocity *ratio* between the center and edges of the cavity remains almost constant** at low and moderate etch depths (Figure S2 in SI). This means that the ratio in surface film thickness should also remain constant. Consequently, the ratio of the limiting current density between center and middle remains constant, which means the second explanation must be responsible for the observed increase in EF with increasing flow rate. The **larger absolute differences** in flow velocity between center and edges at higher flow rate (factor of 5 – 10 (Fig. 4)) cause a larger gradient in surface film thickness, as it is visualized in the bottom parts of Fig. 9a and b. At higher flow rate, a specific change in current density (or potential) results in a narrower part of the cavity reaching the threshold value for etching with the new mechanism, Δx decreases as indicated by the solid (low flow rate) and the dashed (high flow rate) purple curve in Fig. 9b (the same is true for the blue, green, yellow and cyan dashed curves in Fig. 9b). This has a double positive effect: a higher current density in this part and a more localized and directed etching. The optimum current density, which is around 40 A cm^{-2} in our case, shifts to higher current

densities with increasing flow rate. Even higher EF are accessible.

Compared to the 100 µm cavities, the 150 µm cavities exhibit a larger flow velocity ratio between center and edges (compare Fig. 4 with Figure S3 in SI). This results in a lower relative limiting current density at the edges and therefore higher current densities in the regions etching with the new mechanism. Additionally, the gradient in flow velocity (and therefore surface film thickness) is larger compared to the 100 µm cavities, which results, similar to higher flow rates using the 100 µm cavities, in a narrowing of the regions etching with the new mechanism. The addition of both effects explains the significant increase in EF for the 150 µm cavities (Fig. 6).

Similar amplification effects would be expected by intrinsically higher current densities in the center of the cavity, which should also result in more anisotropic etching. However, in narrow cavities exhibiting such a beneficial current density distribution, the flow conditions are likely to be less beneficial for anisotropic etching. This is probably the case for the 50 µm cavities, where the beneficial intrinsic current distribution [21] is superimposed by detrimental hydrodynamic conditions (Figure S4 in SI). The low EF suggests that the probably lower surface film thickness at the edges compensates for the beneficial intrinsic current distribution. This behavior illustrates the strong interplay between intrinsic current distribution and flow conditions regarding the preferred sites of change in mechanism and therefore the resulting anisotropy.

As the etching proceeds and the etch depth increases, the electrolyte flow within the 100 µm cavity becomes more homogeneous (Fig. 4). The positive impact of the increased flow velocity in the center at low etch depths diminishes and ultimately disappears entirely. As a result, the change in mechanism occurs more simultaneously within the entire cavity, Δx increases at given current density, explaining the less anisotropic etching with increasing etch depth (Fig. 6a).

The observed correlation between EF and aspect ratio of the opening (Fig. 6b) is most likely only valid for cavities with comparable current distribution and flow conditions. At very small $AR_{opening}$ ($<< 0.2$) a different behavior would be expected, as illustrated in Fig. 9c. Intrinsically, a higher current density at the edges is expected [21] (black curve in Fig. 9c), which is superimposed by homogeneous flow conditions (Figure S5 in SI) at the limiting current density (red curve in Fig. 9c). At overlimiting current densities, the change in mechanism occurs at first at the edges (blue curve in Fig. 9c). [22] With increasing current density (green, purple and yellow curves in Fig. 9c) the part etched with the new mechanism propagates towards the center of the cavity until at very high current densities (cyan curve in Fig. 9c) the intrinsic current distribution is reached again, when the entire cavity is etched with the new mechanism. For such cavities, the worst EF would be expected at medium overlimiting current densities, whereas a maximum EF should result from etching at the limiting current density. A generally lower EF level compared to small cavities is expected. This assumption agrees well with the observations of Dikusar et al. They obtained the highest EF right at the limiting current density, with cavities exhibiting an $AR_{opening} < 0.1$. [18]

The current density of 5 A cm^{-2} in Fig. 5 is a special case, as the limiting current density is roughly in this range. This is seen clearly in Fig. 3, where a current density of approximately 5 A cm^{-2} is observed between 5 and 24 V for a flow velocity of 4 m s^{-1}. Figs. 3 and 5 are closely linked, especially for this case, and must be considered together. At the lowest flow velocity, the process voltage is high during the entire experiment, meaning a surface film is present leading to a slightly increased anisotropy as compared to all experiments at 2.5 A cm^{-2} and the experiments at 5 A cm^{-2} at higher electrolyte flow. The limited convection is too weak to effectively wash away the surface film. The change in mechanism occurs only at the best flushed position in the middle of the cavity. However, due to the low absolute applied current density the etch rate is only slightly increased compared to the parts etched with the limiting current density (corresponding to the orange curve in Fig. 9a).

For the higher flow rates (at 5 A cm^{-2}), the process voltage drops during the experiment (corresponding to a switch from part III to I in Fig. 3), as the current density drops to below the limiting current density. The current density is slightly decreasing with increasing etch depth due to the increasing active area. This very slight change in current density can lead to a huge drop in voltage, as can be seen in Fig. 3. This results in the loss of the surface film and, consequently, the disappearance of the connected beneficial effect of localized change in mechanism. Contrary to the other current densities, this leads to a decrease in EF with increasing flow rate. This illustrates the importance of the copper nitrate surface film for anisotropic etching and emphasizes, that the mass transport conditions (electrolyte flow velocities at different positions in the etch groove) alone are not sufficient to explain the obtained results. Current density, electrolyte flow and composition and sample geometrical factors need to be carefully balanced to achieve the desired process result.

Another argument supporting the postulated theory is the use of a wetting agent. As the grooves still exhibit smooth surfaces and the process voltage is still comparably high, the wetting agent does not hinder the formation of the surface film. Instead, it eliminates the differences in surface film thickness between the center and edge by mediating between the surface film and the bulk electrolyte (i.e., it facilitates the intermixing of bulk electrolyte and surface film). As the wetting agent concentration increases, the surface film thicknesses at the center and edge equalize, similar to cavities with homogeneous flow conditions (e.g., at large etch depths). The change in mechanism occurs more simultaneously and causes less anisotropic etching. These findings highlight again that the differences in surface film thickness, rather than the beneficial flow conditions alone, lead to highly anisotropic etching. At low current densities, in the absence of a surface film (confirmed by process voltage below 3 V), the wetting agent does not affect the anisotropy of the etching. (Figure S6 in SI)

The plateau region (part II in Fig. 3) is not covered by this study as the experiments were conducted under current control.

4. Conclusions

In this contribution, we presented a consistent set of experiments analyzing the influence of several process parameters in TMEMM on the anisotropy of the etching process, while keeping the other parameters constant. We presented, for the first time, a comprehensive theory explaining the observed results, which significantly extends explanations already present in the literature and connects to the recently published model on reaction mechanisms during high-rate copper dissolution. [22] This theory includes the impact of the local change in mechanism and, therefore, indirectly, of supersaturated surface films on the anisotropy of the etching process. The thickness of the surface film, together with the intrinsic current distribution, determines the localization of the change in mechanism and, therefore, locally strongly increased etching rates. A large gradient in surface film thickness between the center (thin) and edges (thick) is desirable for high anisotropy. This leads to a very beneficial effect at low etch depths, high flow rates, and medium $AR_{opening}$ (around 0.5), which is reduced at high etch depths, very high current densities, and large $AR_{opening}$. At small $AR_{opening}$ ($<< 0.2$), the reverse effect is expected. To ensure comparability of results regarding anisotropy, it is, therefore, important to control and report the etch depth, the aspect ratio of the opening and the limiting current density. A possible solution to reduce the detrimental effect at high etch depths is the application of an impinging electrolyte flow, which enables additionally even higher EF. [5] To enhance the differences in surface film thickness between the center and edges, and therefore improve the anisotropy, an electrolyte additive leading to shear thinning behavior could be added. Further investigations will include the analysis of other electrolytes, exhibiting different etching behavior, e.g., sodium chloride or sodium sulfate. It is expected that the postulated model can, in principle, be transferred to other metals and

electrolytes.

CRediT authorship contribution statement

Leonie Jakob: Writing – original draft, Visualization, Methodology, Investigation, Formal analysis, Data curation, Conceptualization. **Jonas Bartsch:** Writing – review & editing, Visualization, Supervision, Project administration, Funding acquisition.

Declaration of competing interest

The authors declare that they have no known competing financial interests or personal relationships that could have appeared to influence the work reported in this paper.

Acknowledgements

This work was funded by the German Federal Ministry of Economics and Climate Action (BMWK) based on a decision of the German Bundestag under contract number 033EE1053A (PEnELope). The authors would like to thank CONTAG AG for the supply of samples.

Supplementary materials

Supplementary material associated with this article can be found, in the online version, at doi:10.1016/j.electacta.2024.145366.

Data availability

Data will be made available on request.

References

[1] S. Mahata, S. Kunar, B. Bhattacharyya, Fabrication of different micro patterned arrays by through mask electrochemical micromachining, J. Electrochem. Soc. 166 (2019) E217–E225, https://doi.org/10.1149/2.0131908jes.
[2] P. Raffelstetter, B. Mollay, On the modeling of shape evolution in through-mask electrochemical micromachining of complex patterned substrates, Electrochim. Acta 55 (2010) 2149–2157, https://doi.org/10.1016/j.electacta.2009.11.049.
[3] P. Raffelstetter, B. Mollay, B. van den Bossche, G.E. Nauer, Modeling strategy for predicting current density distributions on pcbs and other complex patterned substrates, J. Electrochem. Soc. 156 (2009) D51, https://doi.org/10.1149/1.3033523.
[4] J. Singh, V.K. Jain, J. Ramkumar, Fabrication of complex circuit on printed circuit board (PCB) using electrochemical micro-machining, Int. J. Adv. Manuf. Technol. 85 (2016) 2073–2081, https://doi.org/10.1007/s00170-015-7817-4.
[5] L. Jakob, J. Eckert, C. Podevijn, S. Kluska, M. Junginger, C. Ranzinger, J. Bartsch, Improved uniformity and anisotropy of through-mask electrochemical micromachining by localized etching and homogeneous flow, Int. J. Adv. Manuf. Technol. 130 (2024) 995–1002, https://doi.org/10.1007/s00170-023-12677-3.
[6] X. Chen, N. Qu, X. Fang, Zhu Di, Reduction of undercutting in electrochemical micro-machining of micro-dimple arrays by utilizing oxygen produced at the anode, Surface Coat. Technol. 277 (2015) 44–51, https://doi.org/10.1016/j.surfcoat.2015.07.028.
[7] X. Zhang, N. Qu, H. Li, Z. Xu, Investigation of machining accuracy of micro-dimples fabricated by modified microscale pattern transfer without photolithography of substrates, Int. J. Adv. Manuf. Technol. 81 (2015) 1475–1485, https://doi.org/10.1007/s00170-015-7283-z.
[8] G. Wang, S. Jiang, S. Ni, Y. Zhang, Effect of the mask geometry on the microstructure forming in through-mask electrochemical micromachining, Int. J. Adv. Manuf. Technol. 126 (2023) 3339–3351, https://doi.org/10.1007/s00170-023-11306-3.
[9] C. Madore, Through-mask electrochemical micromachining of Titanium, J. Electrochem. Soc. 146 (1999) 2526, https://doi.org/10.1149/1.1391966.
[10] R.V. Shenoy, Effect of mask wall angle on shape evolution during through-mask electrochemical micromachining, J. Electrochem. Soc. 143 (1996) 544, https://doi.org/10.1149/1.1836477.
[11] T. Baldhoff, V. Nock, A.T. Marshall, Review—through-mask electrochemical micromachining, J. Electrochem. Soc. 165 (2018) E841–E855, https://doi.org/10.1149/2.1341814jes.
[12] M.M. Lohrengel, K.P. Rataj, T. Münninghoff, Electrochemical machining—mechanisms of anodic dissolution, Electrochim. Acta 201 (2016) 348–353, https://doi.org/10.1016/j.electacta.2015.12.219.
[13] M.M. Lohrengel, I. Klüppel, C. Rosenkranz, H. Bettermann, J.W. Schultze, Microscopic investigations of electrochemical machining of Fe in NaNO3, Electrochim. Acta 48 (2003) 3203–3211, https://doi.org/10.1016/S0013-4686(03)00372-4.
[14] L. Jakob, F.D. Heinz, E. Nezam, B. Butschke, I. Krossing, J. Bartsch, In-situ evidence for the existence of surface films in electrochemical machining of Copper in nitrate electrolytes, accepted for publication in Electrochmica Acta (2024).
[15] M. Datta, D. Landolt, On the role of mass transport in high rate dissolution of iron and nickel in ECM electrolytes—II. Chlorate and nitrate solutions, Electrochim. Acta 25 (1980) 1263–1271, https://doi.org/10.1016/0013-4686(80)87131-3.
[16] S.H. Glarum, J.H. Marshall, The anodic dissolution of copper into phosphoric acid: i voltammetric and oscillatory behavior, J. Electrochem. Soc. 132 (1985) 2872–2878, https://doi.org/10.1149/1.2113686.
[17] R. Alkire, H. Deligianni, The role of mass transport on anisotropic electrochemical pattern etching, J. Electrochem. Soc. 135 (1988) 1093–1100, https://doi.org/10.1149/1.2095882.
[18] A.I. Dikusar, O.O. Redkozubova, S.P. Yushchenko, L.B. Kriksunov, D. Harris, Role of hydrodynamic conditions in the distribution of anodic dissolution rates in cavity etching regions during electrochemical micromachining of partially insulated surfaces, Russ. J. Electrochem. 39 (2003) 1073–1077, https://doi.org/10.1023/A:1026167219224.
[19] M. Datta, Fabrication of an array of precision nozzles by through-mask electrochemical micromachining, J. Electrochem. Soc. 142 (1995) 3801–3805, https://doi.org/10.1149/1.2048416.
[20] A.C. West, Shape changes during through-mask electrochemical micromachining of thin metal films, J. Electrochem. Soc. 139 (1992) 499, https://doi.org/10.1149/1.2069245.
[21] R.V. Shenoy, Investigation of island formation during through-mask electrochemical micromachining, J. Electrochem. Soc. 143 (1996) 2305, https://doi.org/10.1149/1.1836997.
[22] L. Jakob, J. Bartsch, I. Krossing, Reaction mechanisms of high-rate copper dissolution in nitrate electrolytes, submitted to Angewandte Chemie International Edition (2024).
[23] A.R. Davis, C. Chong, Laser Raman study of aqueous copper nitrate solutions, Inorg. Chem. 11 (1972) 1891–1895, https://doi.org/10.1021/ic50114a031.
[24] M. Schneider, M. Lohrengel, Electrochemical machining, in: C. Breitkopf, K. Swider-Lyons (Eds.), Springer Handbook of Electrochemical Energy, Springer, Berlin Heidelberg, Berlin, Heidelberg, 2017, pp. 941–971.